Identifying the role of non-adiabatic passing electrons in ITG/TEM microturbulence by comparing fully kinetic and hybrid electron simulations

2012 J. Phys.: Conf. Ser. 401 012006

(http://iopscience.iop.org/1742-6596/401/1/012006)

Journal of Physics: Conference Series **401** (2012) 012006 doi:10.1088/1742-6596/401/1/012006

Identifying the role of non-adiabatic passing electrons in ITG/TEM microturbulence by comparing fully kinetic and hybrid electron simulations

J Dominski[1], S Brunner[1], S K Aghdam[1], T Görler[2], F Jenko[2], and D Told[2]

[1] Centre de Recherches en Physique des Plasmas, Association EURATOM-Confédération Suisse, Ecole Polytechnique Fédérale de Lausanne, CH-1015 Lausanne, Switzerland.
[2] Max-Planck-Institut für Plasmaphysik, EURATOM Association, Boltzmannstrasse 2, D-85748 Garching, Germany.

E-mail: julien.dominski@epfl.ch

Abstract. The response of passing electrons in Ion Temperature Gradient (ITG) and Trapped Electron Mode (TEM) microinstability regimes is investigated in tokamak geometry making use of the flux-tube version of the gyrokinetic code GENE [Jenko *et al.* 2000 *Phys. Plasmas* **7** 1904]. Results are obtained with two different electron models: 1) fully kinetic, and 2) hybrid, in which passing particles are forced to respond adiabatically while trapped are handled kinetically. Comparing linear eigenmodes obtained with these two models enables to systematically isolate radially fine structures located at corresponding MRS's, clearly resulting from the non-adiabatic passing electron response. The analysis of preliminary non-linear simulations in the ITG regime shows that these fine structures on the non-axisymmetric modes survive in the turbulent phase. Furthermore, through non-linear coupling to axisymmetric modes, they induce modulations in the effective density and ion/electron temperature profiles: flattening at low order MRS's and steepening in between, as was already observed in Ref. [Waltz *et al.*, 2006 *Phys. Plasmas* **13** 052301].

1. Introduction

When studying Ion Temperature Gradient (ITG) and Trapped Electron Mode (TEM) microinstabilities and associated turbulence in magnetic fusion devices, it is often assumed that the frequency of the modes are sufficiently low such that the highly mobile *passing* electrons are responding adiabatically. The reduced adiabatic response for passing electrons has thus been extensively applied in gyrokinetic simulations of turbulent transport in the ITG/TEM regime. This approximation is indeed practical due to this important time scale separation between the ion and electron dynamics, such that carrying out simulations resolving the full kinetic evolution of all species remains a great numerical challenge.

The assumption of adiabatic response for the passing electrons is based on the argument that these particles are highly mobile in their motion along the magnetic field line, in such a way that the parallel phase velocity $\omega_r/k_\parallel$ of ITG/TEM microinstabilities is small compared to the electron thermal velocity $v_{th,e}$: $|\omega_r/k_\parallel| \ll v_{th,e}$, where ω_r is the (real) frequency of the mode and $k_\parallel$ its local wavevector component parallel to the magnetic field. However, it turns

out that near low order Mode Rational Surfaces (MRS's) in a toroidal magnetized plasma, the adiabatic passing electron model is in fact not justified. Let us recall that a low order MRS is a surface at which the safety factor q_s is rational, $q_s = -m/n$, with m, n integer, and n a typical toroidal mode number of the considered instabilities (ITG/TEM in our case). At such a MRS, corresponding resonant Fourier modes, *i.e.* with poloidal-toroidal mode number pairs (m, n) such that $q_s = -m/n$, align with the magnetic field line and the associated parallel phase velocity $\omega/k_{\|}$ becomes larger than the electron thermal velocity $v_{th,e}$ within a radial width Δx around this surface. The condition for adiabatic response is thus violated within this interval.

Linear simulations of low frequency microinstabilities have shown that, as a consequence of the non-adiabatic response of passing electrons near MRS's, fine radial structures may form on the fields (e.g. electrostatic potential) of associated eigenmodes within the radial width Δx [1, 2]. The effect of this non-adiabatic electron response near MRS's in the non-linear turbulent regime and its repercussions on associated transport has however barely been addressed in the literature. To our knowledge, this subject has only been partly covered in Ref. [3].

Here, we present first results of a more systematic study of the non-adiabatic electron response in the vicinity of MRS's. This analysis is based on results obtained using the gyrokinetic GENE code [4] considering the simplest possible system. Despite the fact that GENE is a very comprehensive code, which in particular has been generalized more recently to enable global (finite $\rho^\star$) simulations [5], the flux-tube (*i.e.* local) version is considered for this study. Indeed, although all other profiles (temperature/density and their gradients, magnetic geometry coefficients) are assumed constant in the flux tube model, this local representation accounts for the (linearized) variation of the safety factor profile $q_s(x)$ and thus enables to address the particular dynamics in the vicinity of MRS's. Furthermore, a tokamak geometry with circular, concentric magnetic surfaces is chosen, described by the so-called analytic *ad hoc* model [6]. Let us finally point out that all simulations considered in this paper have been are carried out in the electrostatic limit.

The rest of this paper is organized as follows. In Sec. 2, general aspects of the GENE code are briefly described. Section 3 then presents the three different electron models implemented in GENE: 1) the fully kinetic, 2) the (fully) adiabatic, and 3) a hybrid electron model in which the trapped particles are described kinetically, while the passing ones are forced to respond adiabatically. Comparing simulation results from this later model with corresponding fully kinetic electron results provides a systematic way for identifying non-adiabatic passing electron effects. In Sec. 4, a simple analytical estimate for the radial width Δx of the non-adiabatic region around MRS's is derived. In Sec. 5, this theoretical estimate is then compared to the width of fine structures appearing in linear GENE simulations of ITG and TEM eigenmodes. To what extent these fine structures survive in the non-linear regime is then addressed in Sec. 6, where preliminary results of ITG microturbulence have been analyzed. The appearance of regular structures around MRS's on the flux-surface- and time-averaged fields, as a result of non-linear coupling with the unstable modes, is observed, in particular leading to flattening of density and temperature profiles. Conclusions are finally drawn in Sec. 7.

2. The GENE code

GENE evolves the distributions of an arbitrary number of different particle species by solving the associated gyrokinetic equations [7]. It makes use of an Eulerian-based representation and enables to carry out linear and non-linear simulations of microinstabilities and related turbulence in magnetic confinement devices. The system of gyrokinetic equations is closed with reduced Maxwell's equations for the electromagnetic potentials: the quasi-neutrality (or Poisson's) equation is sufficient if only electrostatic fluctuations are considered, while Ampère's law is invoked in addition if electromagnetic fluctuations are accounted for. More details on the system of gyrokinetic equations implemented in GENE can be found in Refs. [5, 8, 9].

In view of presenting the simulation results in Secs. 5 and 6, let us still briefly describe the configuration space coordinates considered in GENE: The code makes use of a field-aligned coordinate system (x, y, z), which is the natural choice for representing the fluctuating fields of microturbulence, themselves aligned with the equilibrium magnetic field $\vec{B}_0$ ($\vec{B}_0 \parallel \nabla x \times \nabla y$). For a tokamak configuration, in terms of the magnetic coordinates (ψ, χ, φ) = (poloidal magnetic flux, straight field line poloidal angle, toroidal angle), one defines the radial coordinate x as an appropriate function of ψ with units of length, the bi-normal coordinate $y = C_y[q_s(\psi)\chi - \varphi]$, and the "parallel" coordinate $z = \chi$. For flux-tube simulations, one chooses $C_y = x_0/q_s(0)$, where x_0 and $q_s(0)$ are respectively the minor radius and safety factor at the flux-tube center, so that y acquires units of length as well. In the coordinates (x, y, z), the flux-tube can then be expressed as a simple rectangular box of size $L_x \times L_y \times L_z$, where $L_z = 2\pi$.

3. Electron Models in GENE

We shall briefly describe here the implementation of the hybrid electron model, a new feature in GENE, which is a reduced description for the electron dynamics in which the trapped particles are described kinetically, while the passing particles are forced to respond adiabatically. This model is clearly only applicable for electrostatic fluctuations, such as ITG/TEM, as it is unable to account for fluctuations in the current carried by passing electrons, which are essential for describing electromagnetic modes. In the frame of the hybrid model, the Quasi-Neutrality Equation (QNE) is thus the only field equation that needs to be accounted for. Let us recall the form taken by the QNE in the fully kinetic and adiabatic description, before introducing its form in the hybrid approach.

3.1. Fully Kinetic

The starting form of the QNE simply reads:

$$\sum_{j=\text{ions},\,\text{e}^-} q_j\, \rho_{1,j}(\vec{x}, t) = 0, \tag{1}$$

where $\rho_{1,j}(\vec{x}, t)$ is the fluctuating part of the density field of species j (here considering one ion species and electrons). Written in terms of the fluctuating part of the gyroaveraged particle distributions $f_{1,j}(\vec{X}, v_\parallel, \mu)$, expressed in gyrocenter variables $(\vec{X}, v_\parallel, \mu)$ [7], the QNE (1) becomes:

$$\sum_{j=\text{ions},\,\text{e}^-} \left\{ \frac{2\pi q_j}{m_j} \int B^\star_{0,\parallel} \bar{f}_{1,j} dv_\parallel d\mu - \frac{q_j^2 n_{0,j}}{T_{0,j}} \left[\phi_1 - \frac{B_0}{T_{0,j}} \int \bar{\bar{\phi}}_1 \exp(-\frac{\mu B_0}{T_{0,j}}) d\mu \right] \right\} = 0, \tag{2}$$

where m_j and q_j are respectively the mass and electric charge of species j, B_0 the equilibrium magnetic field amplitude, and $B^\star_{0,\parallel}/m_j$ the Jacobian of the transformation from particle phase space variables $(\vec{x}, \vec{v})$ to gyrocenter variables $(\vec{X}, v_\parallel, \mu)$. The background density and temperature of each species are noted $n_{0,j}$ and $T_{0,j}$ respectively, while the fluctuating electrostatic potential is given by ϕ_1. As appearing in Eq. (2), the charge density of each species is decomposed into two contributions: the gyrodensity, explicitely expressed in terms of f_1, and the polarization drift, expressed in terms of ϕ_1. The notation $\bar{\mathcal{A}}$ stands for the average of the field $\mathcal{A}(\vec{x})$ over the gyroangle θ (so-called gyroaverage):

$$\mathcal{A}(\vec{X}, \mu) = \frac{1}{2\pi} \oint d\theta \mathcal{A}(\vec{X} + \vec{r}(\theta)),$$

where $\vec{r}(\vec{X}, \mu, \theta)$ is the gyroradius. The field $\bar{\bar{\phi}}_1$, appearing in the polarization drift terms, corresponds to the double gyroaverage of ϕ_1, which in (2) is furthermore weighted over the

background distribution, assumed Maxwellian. Note that the integral $\int dv_\parallel d\mu$ for computing the gyrodensity term is carried out over the whole velocity space for both ions and electrons. Equation (2) thus corresponds to the fully kinetic electron model requiring the evolution of both the ion and electron distributions.

3.2. Adiabatic

In the (fully) adiabatic model, *all* electrons are forced to respond adiabatically. In this case the QNE reads:

$$\left\{ \frac{2\pi q_j}{m_j} \int B^\star_{0,\parallel} \bar{f}_{1,j} dv_\parallel d\mu - \frac{q_j^2 n_{0,j}}{T_{0,j}} \left[\phi_1 - \frac{B_0}{T_{0,j}} \int \bar{\bar{\phi}}_1 \exp(-\frac{\mu B_0}{T_{0,j}}) d\mu \right] \right\}_{j=\text{ions}} = \frac{e^2 n_{0,e}}{T_{0,e}} (\phi_1 - \langle \phi_1 \rangle_{\text{f.s.}}), \tag{3}$$

where the sum over species on the left hand side of Eq. (2) is now reduced to the sole ion contribution, while the charge density contribution from the adiabatic electron response appears on the right hand side of Eq. (3). The notation $\langle \phi_1 \rangle_{\text{f.s.}}$ stands for average over the magnetic flux surface. For this adiabatic model, there is clearly no need to evolve the gyrokinetic equation for the electron distribution.

3.3. Hybrid

Finally, in case of the hybrid model, the QNE is written:

$$\begin{aligned} &\left\{ \frac{2\pi q_j}{m_j} \int B^\star_{0,\parallel} \bar{f}_{1,j} dv_\parallel d\mu - \frac{q_j^2 n_{0,j}}{T_{0,j}} \left[\phi_1 - \frac{B_0}{T_{0,j}} \int \bar{\bar{\phi}}_1 \exp(-\frac{\mu B_0}{T_{0,j}}) d\mu \right] \right\}_{j=\text{ions}} \\ &= - \left\{ \frac{2\pi q_j}{m_j} \int_{\text{trap}} B^\star_{0,\parallel} \bar{f}_{1,j} dv_\parallel d\mu - \frac{q_j^2 n_{0,j}}{T_{0,j}} \left[\alpha_t \, \phi_1 - \frac{B_0}{T_{0,j}} \int_{\text{trap}} \bar{\bar{\phi}}_1 \exp(-\frac{\mu B_0}{T_{0,j}}) d\mu \right] \right\}_{j=\text{e}^-} \\ &\qquad + (1-\alpha_t) \frac{e^2 n_{0,e}}{T_{0,e}} (\phi_1 - \langle \phi_1 \rangle_{\text{f.s.}}), \end{aligned} \tag{4}$$

where the fluctuating electron charge density on the right hand side of Eq. (4) is formed of two contributions: The term $\{\ldots\}_{j=\text{e}^-}$ from the trapped particles, handled kinetically, and the contribution from the passing particles, handled adiabatically and weighted by the corresponding fraction $(1-\alpha_t)$. At a given position $\vec{x}$, the trapped electron contribution involves velocity integrals $\int_{\text{trap}} dv_\parallel d\mu$ over the trapping region, characterized by $m_e v_\parallel^2/2 + [B_0 - B_{0,\max}]\mu < 0$, where $B_{0,\max}(x)$ is the maximum magnetic field on the magnetic surface $x = \text{const.}$ on which $\vec{x}$ lies. The fraction of trapped particles can be estimated as $\alpha_t = [1 - B_0/B_{0,\max}(x)]^{1/2}$.

In the hybrid model, the electron distribution of trapped particles is clearly required as source to the QNE. This is not the case however for the distribution of passing electrons, whose response is enforced to be adiabatic. It may thus appear that the trapped electron distribution can be neglected. This is in fact not true, as the effective particle trajectories, perturbed by the fluctuating fields associated to the microturbulence, can lead to passing particles becoming trapped and *vice versa*. Consequently, the complete electron distribution must nonetheless be evolved in the hybrid model, according to the same gyrokinetic equation considered in the fully kinetic model, except that the passing particle fraction in this case simply evolves passively, *i.e.* without contributing to the self-consistent field ϕ.

As an illustration, the linear spectra obtained with the GENE code using alternatively the fully kinetic, adiabatic, and hybrid electron model for the real frequency ω_r and growth rate γ of the most unstable mode at each ($\sim$ poloidal) wavenumber k_y are presented in Fig. 1. The physical parameters considered are for case ITG-1, summarized in Table 1. For small

For all cases: concentric circular geometry with $x_0/R = 0.16$, $q_s(0) = 1.4$, and $\hat{s} = 0.8$.						
Case	$\omega_n = R/L_n$	$\omega_{T_e} = R/L_{T_e}$	$\omega_{T_i} = R/L_{T_i}$	$k_{ymin}\rho_i$	$\tau = T_e/T_i$	$\mu = m_i/m_e$
ITG-1	2.22	6.96	6.960	0.3	1	1836
ITG-2	2.0	2.0	6.0	0.3 (0.07)	1 (1)	1836 (400)
TEM-2	3.0	6.0	0.0	0.3	1	1836

Table 1. Physical parameters for the different flux-tube GENE simulations. The local inverse aspect ratio, the safety factor and the magnetic shear at the center of the flux-tube are noted x_0/R, $q_s(0)$, and $\hat{s}$ respectively. The characteristic gradients $\omega_{n,T_e,T_i} = R/L_{n,T_e,T_i}$ for density, and electron/ion temperature are normalized wrt. the major radius R. Values in parenthesis are for non-linear runs if different from linear. Ionization degree $Z = 1$ considered for ions in all cases (Hydrogen plasma).

(a) Full spectrum (b) Zoom

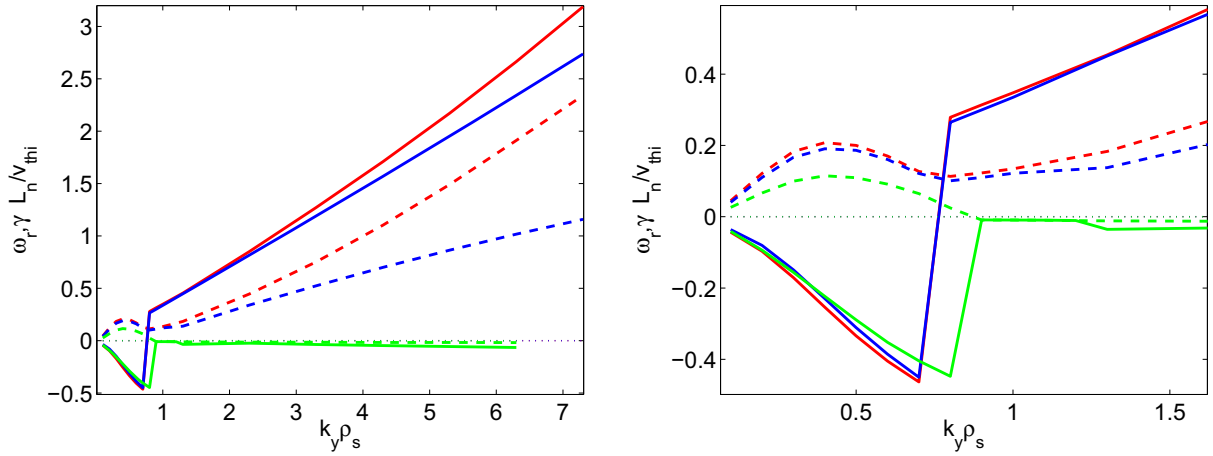

Figure 1. Linear results for Case ITG-1. Comparing the k_y spectra for the real frequency ω_r (full lines) and growth rate γ (dashed) of the most unstable microinstabilities, obtained with the three electron models: fully kinetic (red), adiabatic (green) and hybrid (blue).

wavenumbers, $0 < k_y\rho_i \lesssim 0.7$, the fully kinetic electron model provides an ITG instability ($\omega_r < 0$), well reproduced by the hybrid and approximately reproduced by the adiabatic model. There is indeed a $\sim 30\%$ error on γ with this latter model, resulting from the trapped electrons being forced to respond adiabatically, when in fact they are essentially passive for an ITG. At intermediate wavenumbers, $0.7 \lesssim k_y\rho_i \lesssim 2.0$, the fully kinetic model provides a TEM ($\omega_r > 0$), still well reproduced by the hybrid but absent in the adiabatic model. Finally, at high wavenumbers, $k_y\rho_i \gtrsim 2.0$, the fully kinetic spectra shows a progressive transition of the TEM mode towards an Electron Temperature Gradient (ETG) instability, at which point the hybrid representation starts to fail as well. This example thus clearly summarizes the different ranges of validity for the three different electron models.

4. Analytical Estimate for the Radial Width of Fine Structures

In this section, a simple analytical estimate is derived for the radial width Δx of the regions centered around MRS's, within which the passing electron response is expected to be non-adiabatic.

One considers a given MRS at the radial position $x = x_{m,n}$ such that $q_s(x_{m,n}) = -m/n$ and a

corresponding resonant (poloidal, toroidal) Fourier mode (m, n), component of a microinstability with frequency ω_r. The local wavevector of this Fourier mode is given by $\vec{k} = m\nabla\chi + n\nabla\varphi$ and its component parallel to $\vec{B}_0$ reads:

$$k_\parallel = \vec{k} \cdot \frac{\vec{B}_0}{B_0} = \frac{\vec{B}_0 \cdot \nabla\chi}{B_0}[m + nq_s(x)] \simeq \frac{1}{Rq_s}[m + nq_s(x)],$$

having used $q_s = \vec{B}_0 \cdot \nabla\varphi / \vec{B}_0 \cdot \nabla\chi$, valid for the straight field line poloidal angle χ, and R standing for the major radius of the tokamak. Near the mode rational surface $x = x_{m,n}$, one obviously has $k_\parallel \to 0$ and the condition for adiabatic electron response, $|\omega_r/k_\parallel| \ll v_{th,e}$, breaks down. Taylor expanding around $x = x_{m,n}$ leads to $q_s(x = x_{m,n} + \delta x) \simeq q_s(x_{m,n})[1 + \hat{s}\,\delta x/x_{m,n}]$, as well as

$$k_\parallel(\delta x) = \frac{\hat{s}}{q_s}\frac{\delta x}{R}k_y,$$

where $\hat{s} = (x/q_s)\,dq_s/dx$ stands for the magnetic shear and $k_y = nq_s/x_{m,n}$ is the wavenumber with respect to the direction y (as $m \simeq nq_s$ for field-aligned modes, k_y in fact provides an estimate of the poloidal wavenumber). The region of non-adiabatic electron response is then estimated as $\Delta x = 2\delta x$ such that $\omega_r/k_\parallel(\delta x) = v_{th,e}$, finally providing:

$$\frac{\Delta x^{\mathrm{th}}}{\rho_i} = 2\,\frac{\omega_r}{v_{th,i}/R}\,\frac{q_s}{\hat{s}\,\sqrt{\tau\mu}\,k_y\rho_i}. \tag{5}$$

In this last relation, the width Δx^{th} and the wavenumber k_y have been normalized using the ion Larmor radius ρ_i, while the frequency ω_r is normalized with respect to the reference value $v_{th,i}/R$, where $v_{th,i}$ stands for the ion thermal velocity. Furthermore, $\tau = T_e/T_i$ and $\mu^{-1} = m_e/m_i$ respectively represent the electron/ion temperature and mass ratios. The dependence of Δx^{th} in Eq. (5) on μ obviously reflects the non-adiabatic nature of electrons which is accounted for in this context.

5. Linear Simulations

Linear flux-tube simulations of ITG and TEM eigenmodes have been computed making use of the spectral solver provided in the GENE code. In an axisymmetric system, such as in tokamaks considered here, linear eigenmodes have a fixed toroidal wavenumber n, which in GENE's field-aligned coordinate system (x, y, z) translates to a fixed wavenumber $k_y = n/C_y = nq_s/x_0$. Furthermore, as the unperturbed system is stationary, eigenmodes also have a fixed, complex frequency ω. In the GENE representation, an eigenmodes thus takes on the functional form (illustrated here on the electrostatic potential ϕ):

$$\phi(x, y, z; t) = \hat{\phi}(x, z)\exp[\imath(k_y y - \omega t)].$$

The eigenmode is therefore essentially characterized by the complex amplitude $\hat{\phi}(x, z)$, which represents the slow spatial variation, the fast phase variation being contained in the factor $\exp(\imath k_y y)$.

Figure 2 shows the typical eigenmode envelope $|\hat{\phi}(x, z)|$ for both an ITG and TEM mode, corresponding respectively to cases ITG-2 and TEM-2 of Table 1. The ITG and TEM results appear respectively in the left and right columns of sub-plots. In a linear, flux-tube simulation, due to the imposed periodic boundary conditions in x, the system size L_x along this direction must be taken as the distance between consecutive MRS's for the considered k_y mode number: $1 = n(dq_s/dx)L_x = k_y\hat{s}L_x$, leading to $L_x = 1/(k_y\hat{s})$. For $k_y\rho_i = 0.3$ and $\hat{s} = 0.8$ considered here, one thus obtains $L_x/\rho_i = 4.17$. Furthermore, the flux-tube is centered such that the single MRS

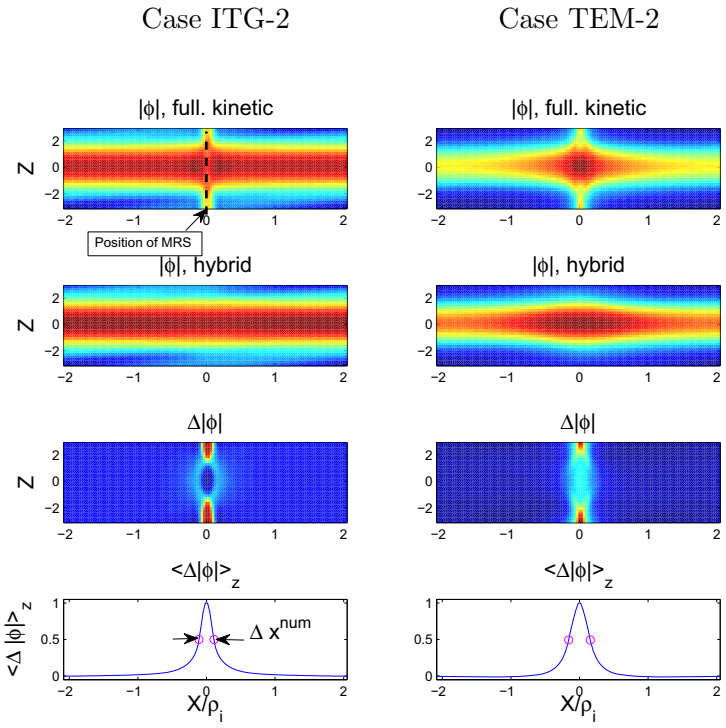

Figure 2. Envelopes $|\hat{\phi}|(x,z)$ of linear eigenmodes for ITG-2 and TEM-2 cases described in Table 1. The MRS for the considered $k_y\rho_i = 0.3$ is positioned at $x = 0$. The first and second row of sub-plots respectively present the results from the fully kinetic and hybrid electron models. The difference $\Delta|\hat{\phi}|$ is shown in the third row and its z-averaged profile in the fourth row, from which the numerical FWHM $\Delta x^{\rm num}$ estimate for the fine structure width can be obtained. Color coding: dark blue = zero, dark red = max. value.

contained in L_x is positioned at $x = 0$. The first row of sub-plots in Fig. 2 presents the results carried out with the fully kinetic model, while the second row shows the results obtained with the hybrid model. Note in all cases the modulation of the eigenmodes with respect to z: a large (resp. low) mode amplitude at $z = 0$ (resp. $z = \pm\pi$) corresponding to the outer (resp. inner) mid-plane of the tokamak, reflecting the characteristic ballooning structure of ITG/TEM modes. A notable difference however is the presence of a fine slab-like (non-ballooned) structure centered at $x = 0$ in the eigenmodes from the fully kinetic model, which is absent in the hybrid model results, thus clearly identified as a feature resulting from the kinetic passing electron dynamics and lying on the MRS's corresponding to the considered k_y. By subtracting the mode envelopes obtained from the two different electron models, $\Delta|\hat{\phi}|(x,z) = |\hat{\phi}^{\rm full.kin.}| - |\hat{\phi}^{\rm hybrid}|$ shown in the third row of sub-plots of Fig. 2, enables to cleanly isolate the structure. Furthermore z-averaging $\Delta|\hat{\phi}|(x,z)$ provides an average radial profile $\langle\Delta|\hat{\phi}|\rangle_z(x)$ shown in the last row of Fig. 2, from which a numerical estimate $\Delta x^{\rm num}$ of the structure width can be measured as the Full Width at Half Maximum (FWHM). The z-average is defined as $\langle . \rangle_z = \int . J dz / \int J dz$, where J is the Jacobian of the (x, y, z) coordinate system.

Estimates for $\Delta x^{\rm num}$ can be obtained while alternatively scanning the different physical parameters τ, μ, q_s, $\hat{s}$, and $k_y\rho_i$, all predicted to affect the fine structures according to the theoretical derivation for $\Delta x^{\rm th}$ leading to Eq. (5). Such scans have been carried out starting from the reference values given in Table 1 and considering both the ITG-2 and TEM-2 cases.

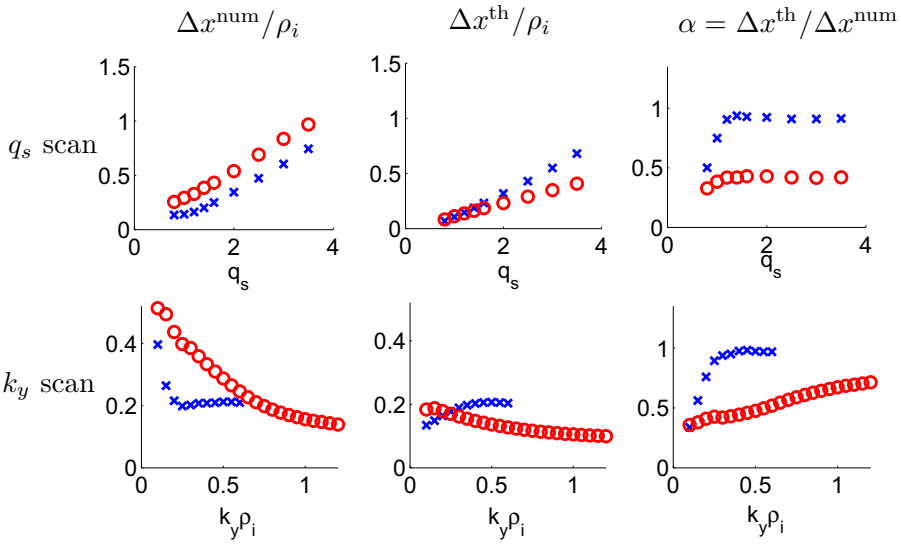

Figure 3. Comparison of the numerical and theoretical estimates, $\Delta x^{\rm num}$ and $\Delta x^{\rm th}$ respectively, for the width of fine structures for linear ITG/TEM modes along scans in the safety factor q_s and wavenumber $k_y\rho_i$. The factor $\alpha = \Delta x^{\rm th}/\Delta x^{\rm num}$ provides a measure of the agreement. Blue crosses: case ITG-2, red circles: TEM-2.

Corresponding results for scans in the safety factor q_s and wavenumber $k_y\rho_i$ are shown in Fig. 3. Note that, for evaluating the theoretical estimate (5) requires the knowledge of the real frequency ω_r of the eigenmode, which is taken from the simulation. Furthermore, the theoretical relation for $\Delta x^{\rm th}$ is based on the assumption that the boundary of the non-adiabatic passing electron response regions starts where the parallel phase velocity $\omega_r/k_\parallel$ equals *exactly* the electron thermal velocity $v_{th,e}$ (See Sec. 4). This is clearly arbitrary, as the transition from adiabatic to non-adiabatic is spatially continuous. In the same way, the numerical estimate $\Delta x^{\rm num}$, defined as the FWHM of $\Delta|\hat{\phi}|$, is ad hoc as well. One thus introduces the adjustment factor $\alpha = \Delta x^{\rm th}/\Delta x^{\rm num}$, which provides a good measure of the agreement between theoretical and numerical results. As shown in Fig. 3, the factor α is approximately constant over a significant range of the considered scans and furthermore takes on values ~ 1, which reflects that the theoretical relation (5) captures the essential parametric scalings and actually provides a good semi-quantitative estimate of the fine radial structures.

6. Non-Linear Simulations

Preliminary non-linear microturbulence results addressing the role of non-adiabatic passing electrons in the turbulent regime are presented here. One considers the case ITG-2, which leads to an ITG-dominated regime. Note that, contrary to the linear runs for which the physical mass ratio $\mu = 1836$ was chosen, the non-linear results were obtained with the reduced mass ratio $\mu = 400$ (see Table 1). Two simulations have again been performed, considering either the fully kinetic or hybrid electron model. These runs have been carried out over a simulation time of more than $150\,R/v_{th,i}$, ensuring good statistics (for reference, the corresponding maximum linear growth rates of the underlying ITG modes are of order $\gamma_{\rm max} \simeq 0.3\,v_{th,i}/R$). Contrary to linear calculations, non-linear runs obviously require to simultaneously account for the full spectrum of k_y modes. In a diagnostic process, one may nonetheless Fourier decompose the

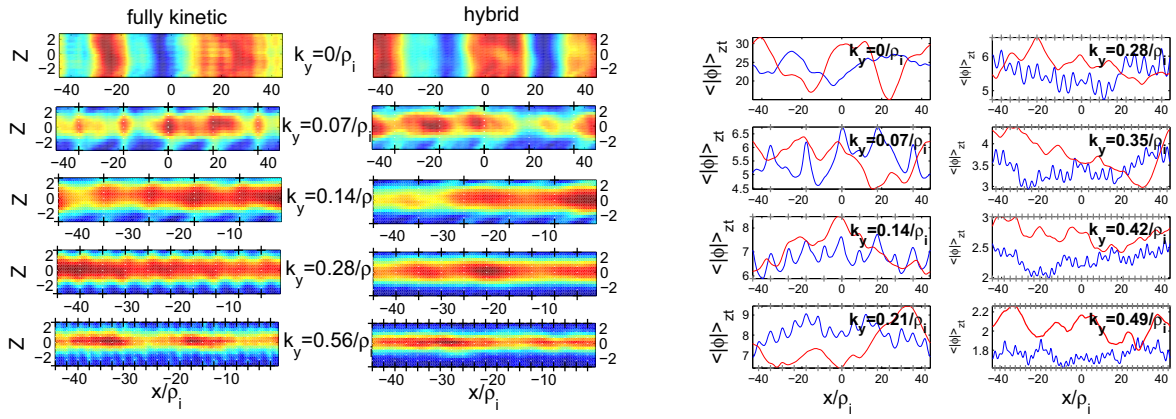

Figure 4. Non-linear ITG-2 case. Comparing results from both the fully kinetic and hybrid electron model. (left) Time-averaged Fourier amplitudes $\langle|\hat{\phi}_{k_y}|\rangle_t(x,z)$ of the electrostatic potential. Showing modes $k_y/k_{y,\min} = 0, 1, 2, 4\,\&\,8$, with $k_{y,\min}\rho_i = 0.07$. (right) Radial profiles of corresponding z-averages $\langle|\hat{\phi}_{k_y}|\rangle_{z,t}(x)$. Showing modes $k_y/k_{y,\min} = 0$ to 7. For each k_y, associated MRS's are pointed out with tick marks along the box edge of the corresponding figure. Blue lines: fully kinetic, red: hybrid electron model.

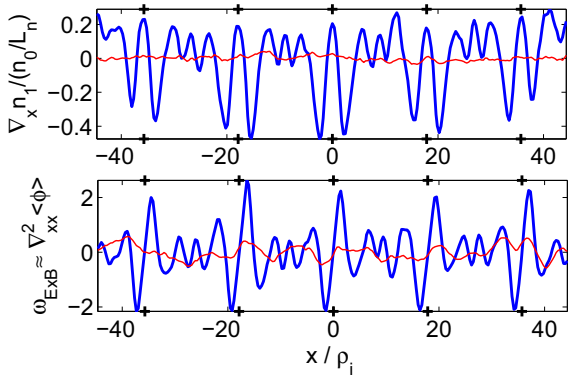

Figure 5. Non-linear ITG-2 case. (Top) Radial profiles of $(d/dx)\langle n_1\rangle_{\text{f.s.,t}}(x)$, where $\langle n_1\rangle_{\text{f.s.,t}}$ is the flux-surface- and time-averaged density fluctuation. (Bottom) Radial profile of the time-averaged $E \times B$ shearing rate $\langle\omega_{E\times B}\rangle_t(x)$ associated with the zonal flows.

turbulent fields and extract the different k_y modes, thus enabling to perform a similar analysis on the corresponding time-averaged mode amplitudes of the electrostatic field, $\langle|\hat{\phi}_{k_y}|\rangle_t(x,z)$, as done for the linear eigenmodes in Sec. 5 ($\langle.\rangle_t$ stands for the time average).

In the radial direction, the system size L_x considered for the non-linear flux-tube simulations must be chosen as an integer multiple of the distance $1/(k_{y,\min}\hat{s})$ separating lowest order MRS's, where the minimum k_y mode number $k_{y,\min}\rho_i = 0.07$ was set for the here considered simulations. The system length L_x must furthermore be significantly larger than the radial correlation length of the turbulence, which typically requires at least $L_x/\rho_i \sim 10^2$. One thus chose $L_x/\rho_i = 5/(k_{y,\min}\rho_i\,\hat{s}) = 89.3$, so that the system encompasses 5 lowest order MRS's. Concerning numerical resolution, $n_x = 256$, $n_y = 32$, and $n_z = 16$ grid points were considered in the x, y, and z-directions respectively. In particular, for the x-resolution one has $L_x/n_x = 0.35\,\rho_i$. This may appear marginal considering the widths of fine structures observed on the linear modes, but turns out to be appropriate for resolving the characteristic structures appearing in the non-

linear simulation as shown in the following. Concerning velocity space resolution, $n_{v_\parallel} = 64$ and $n_\mu = 32$ mesh points were chosen in the $v_\parallel$ and μ directions respectively.

The time-averaged amplitudes of k_y Fourier modes obtained from the electrostatic potential, $\langle|\hat{\phi}_{k_y}|\rangle_t(x,z)$, are shown for the non-linear ITG-2 case simulations in Fig. 4. Also shown are the corresponding z-averages $\langle|\hat{\phi}_{k_y}|\rangle_{z,t}(x)$. For each mode $k_y > 0$, these plots clearly point out the presence in the fully kinetic results of fine radial structures located at the associated MRS's, positioned at $x = \Delta m/(k_y\hat{s})$, Δm integer, and high-lighted with tick marks in the corresponding plots. Similar fine structures are absent in the hybrid simulations, confirming that the non-adiabatic passing electron structures identified in the linear simulations actually persist in the non-linear, turbulent regime. The clean procedure used in the linear study for measuring the radial width of non-adiabatic structures, based on subtraction of fully kinetic and hybrid results, is not applicable in any straightforward way for analyzing the non-linear data. One can nonetheless estimate the widths $\Delta x^{\rm num}$ by directly measuring on $\langle|\hat{\phi}^{\rm full.kin.}_{k_y}|\rangle_{z,t}(x)$ the FWHM of fine structures appearing at each corresponding MRS's. Corresponding results show that the fine structures, although having survived in the non-linear regime, are significantly broadened. For example, at $k_y\rho_i = 0.35$, the linear results (for $\mu = 400$) present a width of order $\Delta x^{\rm num}/\rho_i = 0.45$, while measuring structures on the corresponding mode in the non-linear simulations provides an average value $\Delta x^{\rm num}/\rho_i \simeq 1.7$.

Considering in Fig. 4 the plot depicting $\langle|\hat{\phi}_{k_y}|\rangle_{z,t}(x)$ for $k_y\rho_i = 0$, there seems to be no apparent fine structure in this mode. Naturally, $k_y = 0$ itself has no associated MRS. However, when estimating the time-averaged shearing rate $\omega_{E\times B} = (d/dx)v_{E\times B} = -(1/B)(d^2/dx^2)\langle\phi\rangle_{\rm f.s}$ of $E\times B$ flows associated to the zonal component $\langle\phi\rangle_{\rm f.s} = \int \hat{\phi}_{k_y=0}(x,z)\, J\, dz/\int J\, dz$, clear fine structures with a scale length of a few ion Larmor radii ρ_i centered around the lowest order MRS's appear in the fully kinetic electron simulation, as clearly illustrated in Fig. 5. Such structures are again essentially absent in the results obtained with the hybrid model. The plot for $\langle\omega_{E\times B}\rangle_t$ in Fig. 5 thus is related to the second order derivative of the radial profile $\langle|\hat{\phi}_{k_y=0}|\rangle_{z,t}(x)$ in Fig. 4, the derivatives having accentuated the underlying fine structures in the kinetic runs. Remarkable in the corresponding radial profile of $\langle\omega_{E\times B}\rangle_t(x)$ is the regular pattern of fine structures that appear, periodically repeated over each lowest order MRS interval of length $1/(k_{y,\rm min}\hat{s})$ (positions of lowest order MRS's are again high-lighted in the plot with tick marks). Structures in $\langle\omega_{E\times B}\rangle_t(x)$ are thus clearly aligned with the lowest order MRS's (related to $k_y = k_{y,\rm min}$), presenting an *odd* parity with respect to these radial positions. Similar sub-structures can also be identified at the second order MRS's ($k_y = 2\,k_{y,\rm min}$) as well as third order ones ($k_y = 3\,k_{y,\rm min}$).

In a similar way as has been done for ϕ, one can investigate the flux-surface- and time-average of density and ion/electron temperature fluctuation fields. Considering for example the density fluctuation n_1 (same for ions and electrons as quasi-neutrality is verified), the radial derivative of the corresponding averaged profile, $(d/dx)\langle n_1\rangle_{\rm f.s.,t}(x)$, is also shown in Fig. 5. As for the shearing rate profile $\langle\omega_{E\times B}\rangle_t(x)$, similar structures aligned with the MRS's are found for the fully kinetic model, again absent for the hybrid results. Note however that for $\langle n_1\rangle$, the structures present an *even* parity with respect to the positions of MRS's (to lighten notations one writes here $\langle n_1\rangle$ in place of $\langle n_1\rangle_{\rm f.s.,t}$). In fact, the profile $(d/dx)\langle n_1\rangle(x)$ systematically presents *maxima* at the MRS's. This reflects the tendency towards stationary *flattenings* in the corresponding effective profiles. Indeed, the total stationary density profile reads $n = n_0 + \langle n_1\rangle$ and the condition $dn/dx = 0$ for a flattened region becomes $(L_n/n_0)(d/dx)\langle n_1\rangle = 1$. Values of $(L_n/n_0)(d/dx)\langle n_1\rangle \simeq 0.2$ appearing in Fig. 5 at lowest order MRS's thus correspond to partial flattenings of the density profile. Flattenings are observed as well at the next order MRS's, although weaker on average. Conversely, the profiles are *steepened* between MRS's, reflected by $(L_n/n_0)(d/dx)\langle n_1\rangle$ taking on negative values in the corresponding regions, thus resulting in

an effectively step-like profile. The development of similar step-like profiles is observed for the ion/electron profiles as well (not shown here). These results thus confirm the corrugated profiles already observed in Ref. [3] using the GYRO code.

7. Conclusions

A simple theoretical estimate has been derived for the radial width Δx of non-adiabatic passing electron regions in which fine structures appear on the linear ITG/TEM eigenmodes with $k_y \neq 0$ at corresponding MRS's. This estimate has been successfully validated against numerical results obtained with linear, flux-tube simulations using the GENE code. The theoretical relation for Δx is in particular useful for determining the numerical resolution required for spatially resolving these non-adiabatic structures.

Preliminary results obtained from non-linear, flux-tube simulations in an ITG-dominated scenario have shown that the structures on the different $k_y \neq 0$ modes persist, albeit broadened, in the turbulent regime. Furthermore, through non-linear coupling to the $k_y = 0$ mode, fine structures located around lowest order MRS's also appear in the radial profiles of time- and flux-surface-averaged fluctuating fields, such as density n_1 and ion/electron temperature $T_{1,i/e}$. These structures are such that the associated total profiles show the tendency towards a flattening near low order MRS's and a steepening in between, leading to effective step-like density and temperature profiles, confirming results obtained in Ref. [3]. It should be emphasized that this phenomena of profile flattening near MRS is analyzed here for essentially electrostatic perturbations, and thus involves no electromagnetic fluctuations such as *e.g.* microtearing modes.

The modulation of the effective profile gradients can thus be interpreted as a clear sign that transport of particles and heat is, at least locally, influenced by the particular dynamics of non-adiabatic passing electrons near MRS's. In particular, stationary structures appearing as well on the radial shearing rate profile $\omega_{E\times B}(x)$, associated to the zonal flows, seem to play a key role in sustaining the step-like profiles. Indeed, regions of steepened gradients happen to coincide with regions where $|\omega_{E\times B}|$ is large. This is consistent with the fact that sheared flows effectively break up turbulent eddies, which results in reduced associated transport. Conversely, regions of flattened gradients coincide with low values of $|\omega_{E\times B}|$.

Further investigation of the role of non-adiabatic passing electrons in the vicinity of MRS's on profile evolutions and overall transport processes is clearly required and currently being carried out for both ITG and TEM dominated regimes, and shall be reported on in a future publication.

Acknowledgments

This work was partly supported by the Swiss National Science Foundation. GENE simulations have been carried out on the HPC-FF computer at the Jülich Forschungszentrum, Germany.

References

[1] Falchetto G L, Vaclavik J and Villard L 2003 *Physics of Plasmas* **10** 1424–1436
[2] Chowdhury J, Ganesh R, Angelino P, Vaclavik J, Villard L and Brunner S 2008 *Physics of Plasmas* **15** 072117
[3] Waltz R E, Austin M E, Burrell K H and Candy J 2006 *Physics of Plasmas* **13** 052301
[4] Jenko F, Dorland W, Kotschenreuther M and Rogers B N 2000 *Physics of Plasmas* **7** 1904–1910
[5] Görler T, Lapillonne X, Brunner S, Dannert T, Jenko F, Merz F and Told D 2011 *Journal of Computational Physics* **230** 7053 – 7071 ISSN 0021-9991
[6] Lapillonne X, Brunner S, Dannert T, Jolliet S, Marinoni A, Villard L, Gorler T, Jenko F and Merz F 2009 *Physics of Plasmas* **16** 032308
[7] Brizard A J and Hahm T S 2007 *Rev. Mod. Phys.* **79**(2) 421–468
[8] Görler T 2009 Ph.D. thesis University of Ulm, Germany
[9] Lapillonne X 2010 Ph.D. thesis Ecole Polytechnique Fédérale de Lausanne, Switzerland